

Supplemental Material -

Single Image Object Counting and Localizing using Active-Learning

Inbar Huberman-Spiegelglas Raanan Fattal

`{inbar.huberman1, raanan.fattal}@mail.huji.ac.il`

School of Computer Science and Engineering
The Hebrew University of Jerusalem, Israel

Appendix

Method Pseudo-Code

Algorithm 1 summarizes all the steps of our active-learning process.

Algorithm 1: Method Pseudo-Code.

```

Input : Input image  $I$ , user-marked bounding window  $B$ 
Output: detected repeating object coordinates  $\mathcal{O}$ 
/* initialization
ncc = NCC( $I, B$ )
 $\mathcal{P} = \text{MaxSup}(ncc \geq 0.85), \mathcal{N} = ncc \leq 0$ 
train CNN on  $\mathcal{P}, \mathcal{N}$ 
 $C = \text{CNN}(I)$ 
while not terminated do
     $C^s(\mathbf{x}) = \text{MaxSup}(C(\mathbf{x}))$ 
    /* Extract potential locations
     $\mathcal{W} = \{\mathbf{x} | C^s(\mathbf{x}) > 0\}$ 
    /* Associate potential windows with
       labeled coordinate
     $l_w, d_w = \text{GetNearestLabel}(\mathcal{W}, \mathcal{P}, \mathcal{N})$ 
     $\mathcal{W}^P = \{\mathbf{x} \in \mathcal{W} | l_w = \text{Pos.}\}, \mathcal{W}^N = \{\mathbf{x} \in \mathcal{W} | l_w = \text{Neg.}\}$ 
    /* Clustering each set
     $\Theta^P = Kmeans(\mathcal{W}^P, k=10), \Theta^N = Kmeans(\mathcal{W}^N, k=10)$ 
    /* find most distant windows
     $q_i^P = \text{GetTop5Clust}(\Theta^P, d_w),$ 
     $q_i^N = \text{GetTop5Clust}(\Theta^N, d_w)$ 
    /* User corrections
     $\mathcal{L}^P, \mathcal{L}^N = \text{GetUserInput}(q_i^P, q_i^N)$ 
    /* Updating label sets
     $\mathcal{P} = \mathcal{P} \cup \mathcal{L}^P, \mathcal{N} = \mathcal{N} \cup \mathcal{L}^N$ 
    /* further training
    train CNN on  $\mathcal{P}, \mathcal{N}$ 
     $C = \text{CNN}(I)$ 
 $C^s(\mathbf{x}) = \text{MaxSup}(C(\mathbf{x}))$ 
 $\mathcal{O} = \{\mathbf{x} | C^s(\mathbf{x}) > 0\}$ 

```

Hyper-parameter Search and Ablation Study

In order to search the optimal hyper-parameters as well as to evaluate the contribution of the proposed method components, we set up an “automated” version of our method. In this mode, we use a ground-truth, per-pixel, image labeling in order to provide an automated user feedback, as well as an initial bounding window pointing out the object of interest. This allows us to perform extensive tests over

configuration	NCC				sub-space loss				random querying	cross-entropy
	threshold	m	α	0.5	1.5	2	2.5			
param. values	0.8 +0.62	0.9 +0.69	0.5N +0.97	1.5N +0.91	0 +0.95	0.5 +1.07	1.5 +0.62	2 +0.65	2.5 +0.45	+0.77 +0.45
diff. cnt. err. [%]										

Table 1: Hyper-parameters Search and Ablation Study. Difference in error percentage are reported with respect to changes from the default values used in our method, namely, $\alpha = 1$, $m = N$ and NCC threshold of 0.85.

multiple images. We used ten images to perform this hyper-parameter search and ablation study, none of which appears in the test sets that we report in Table 1 in the paper.

The evaluation of these hyper-parameters is summarized in Table 1 which reports the differences of average counting error percentage when the default values are changed to the ones in the table. The parameters explored are: the NCC threshold at the network initialization step in Section 3.1 (the default value is 0.85), the sub-space separation dimension m from Eq. 3 (default value N), as well as its loss weight α suggested in Section 3.4 (default value 1).

Next we evaluate the benefit obtained by the novel components of our method. By setting $\alpha = 0$ we measure the contribution of the sub-space separation loss which, according to Table 1, reduces the average counting error by 15.7%, from 6.95% to 6% (our method’s performance in the automated mode). The cluster-based query extraction was compared to a random selection of queries from \mathcal{W}^P and \mathcal{W}^N . This test shows a reduction of 12.9%, from 6.78% to 6%, in average counting error. Finally, the use of MSE loss in Eq. 2 instead of a cross-entropy loss reduces the counting error by 6.4%, from 7.4% to 6.95% (when using $\alpha = 0$).

We also evaluated the number of user corrections when presenting all the queries along with a positive tentative labels (following the fact that $C(\mathbf{x}) > 0, \forall \mathbf{x} \in \mathcal{W}$), compared to the labels derived from the association with \mathcal{W}^P or \mathcal{W}^N that we use. This resulted in a reduction of 34% in the average number of user mouse clicks, from 18.5 to 13.8. Note that since both cases consist of the same query extraction scheme, there is no change in the counting error.

Comprehensive Results for User-Study

Below is the full table comparing Artera *et al.* [1], Hieberman and Fattal [3] and our method.

Qualitative Results

Below we present the 33 test images along with our outputs produced by the user-study.

- For each image we present the best result and average result obtained in our user study in terms of localization error
- Our result images are shown in gray-scale and our localizations are indicated in purple dots
- For some images - which appear to be easy for our method to obtain accurate results we show the worst result obtained in the user study (this is indicated in the relevant figures)

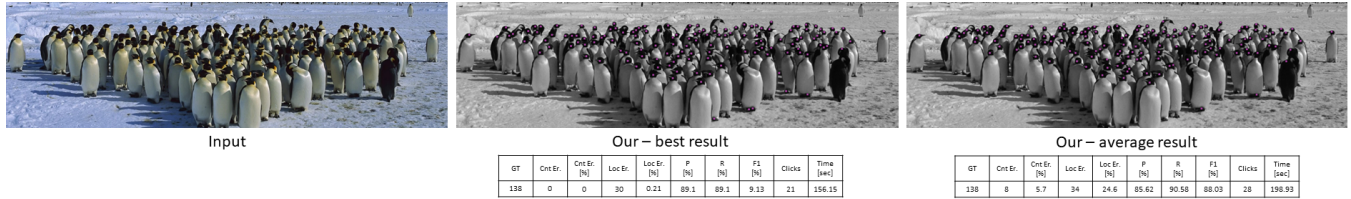


Figure 1: Antarctica.

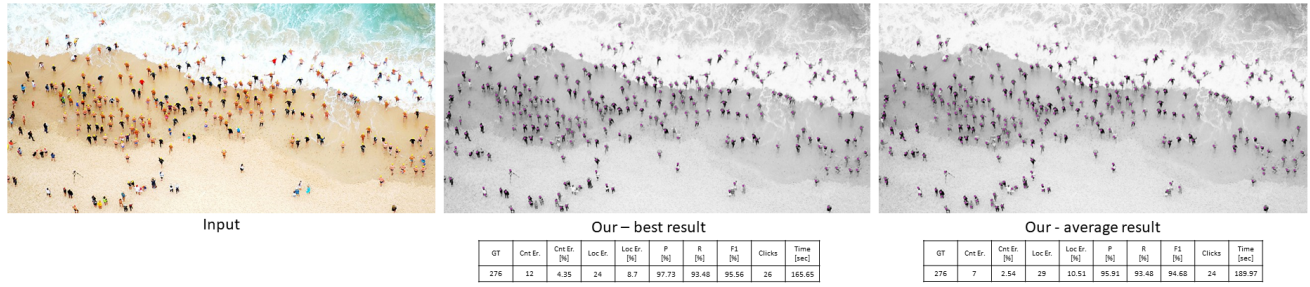


Figure 2: Beach.

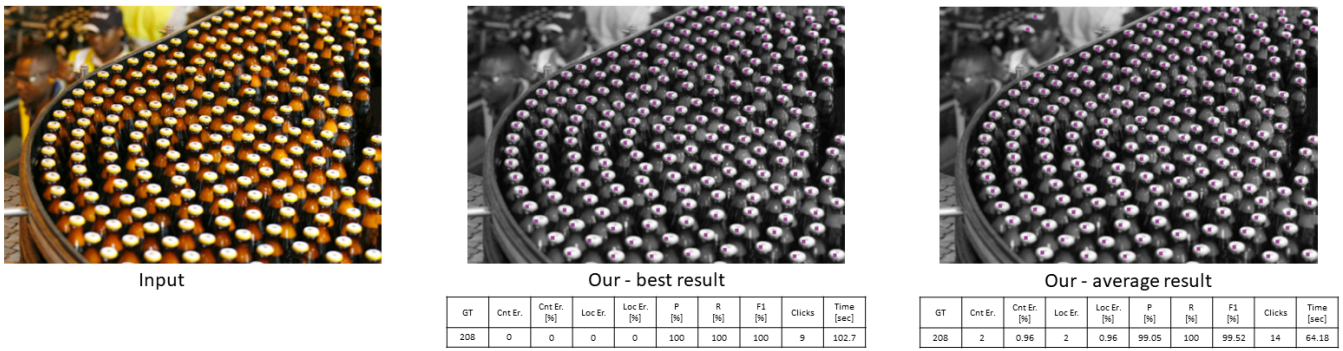


Figure 3: Beer.

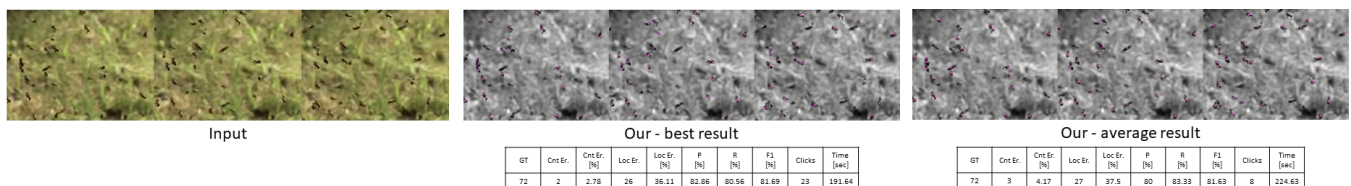


Figure 4: Bees. 3 frames, small object dataset [5]

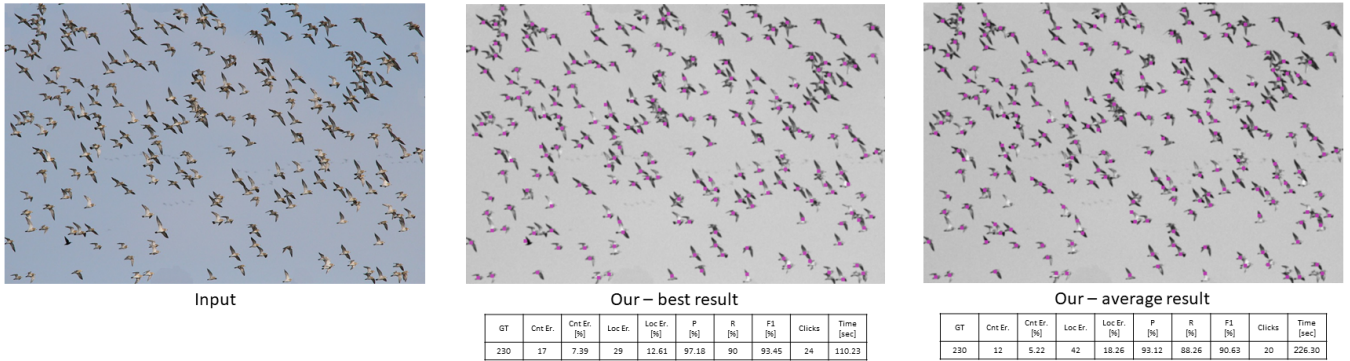


Figure 5: Birds.

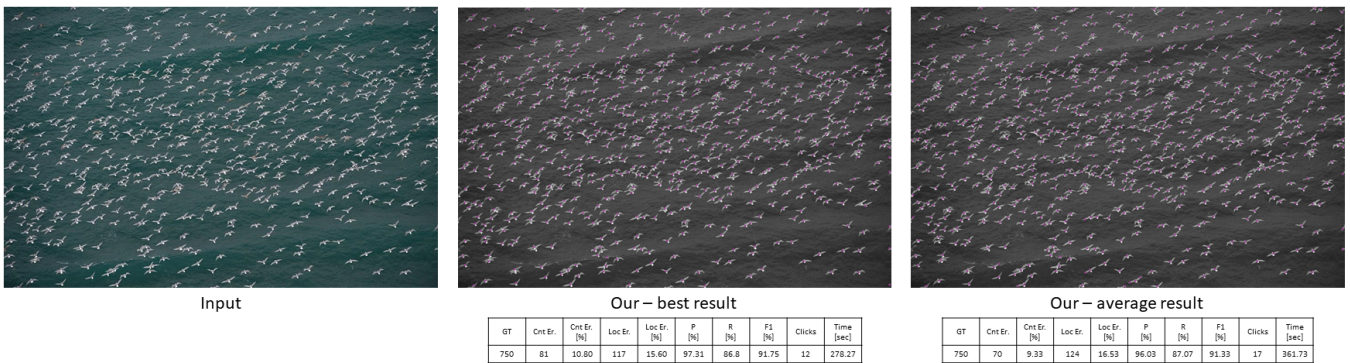


Figure 6: Birds002. small object dataset [5]

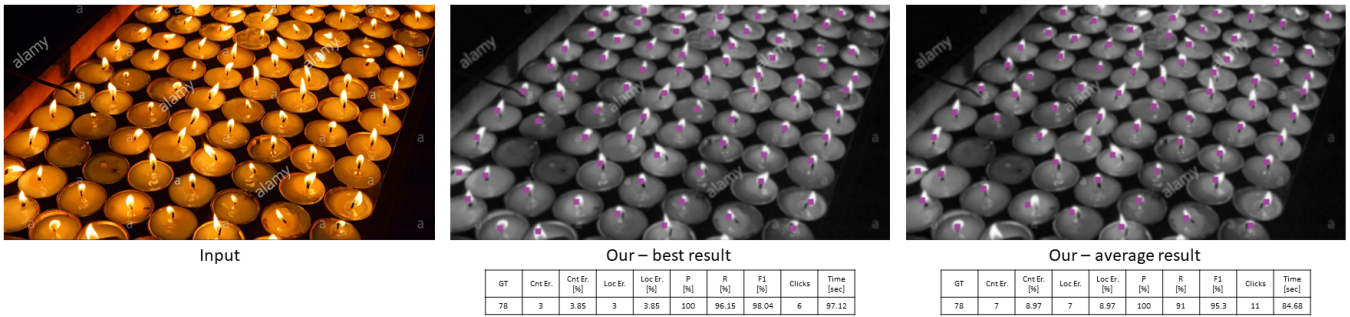


Figure 7: Candles.

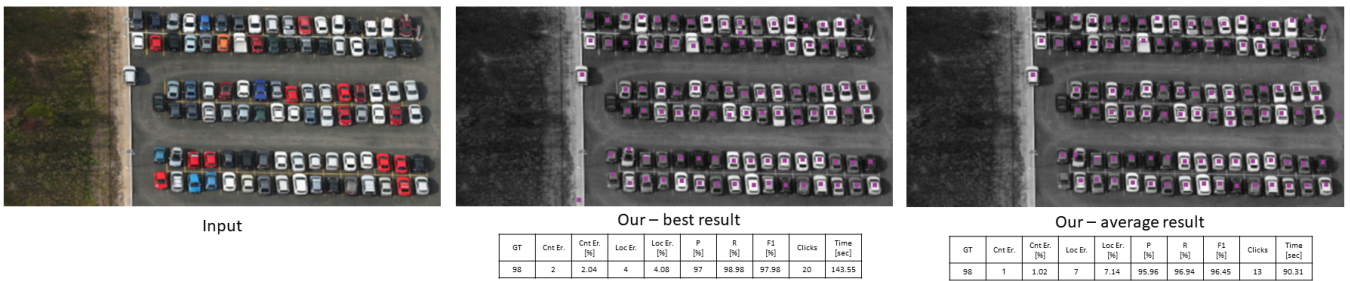


Figure 8: Cars.

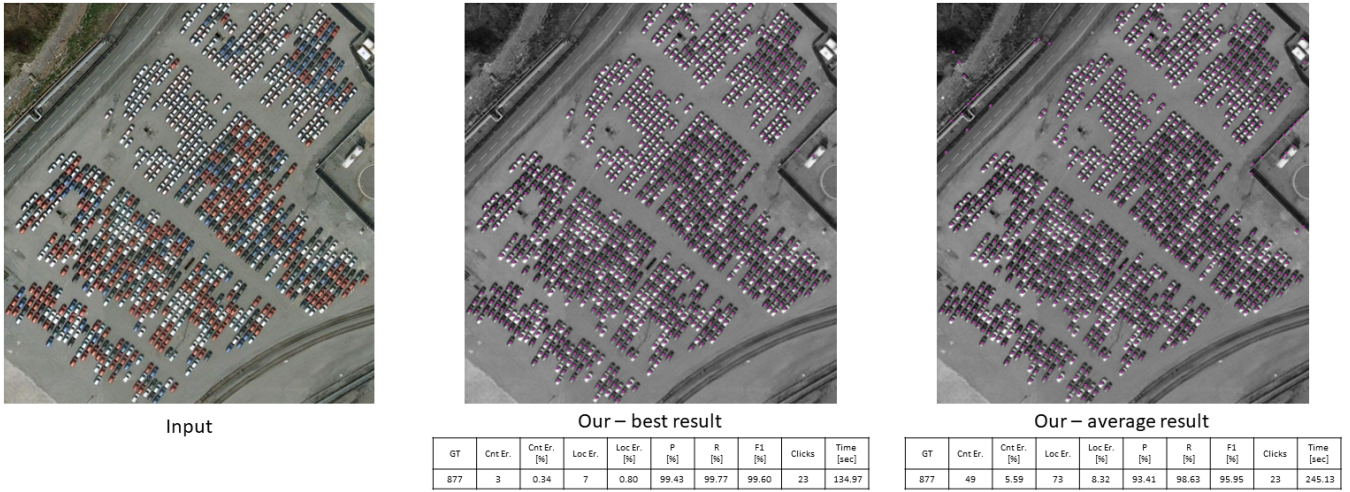


Figure 9: CarsBg.

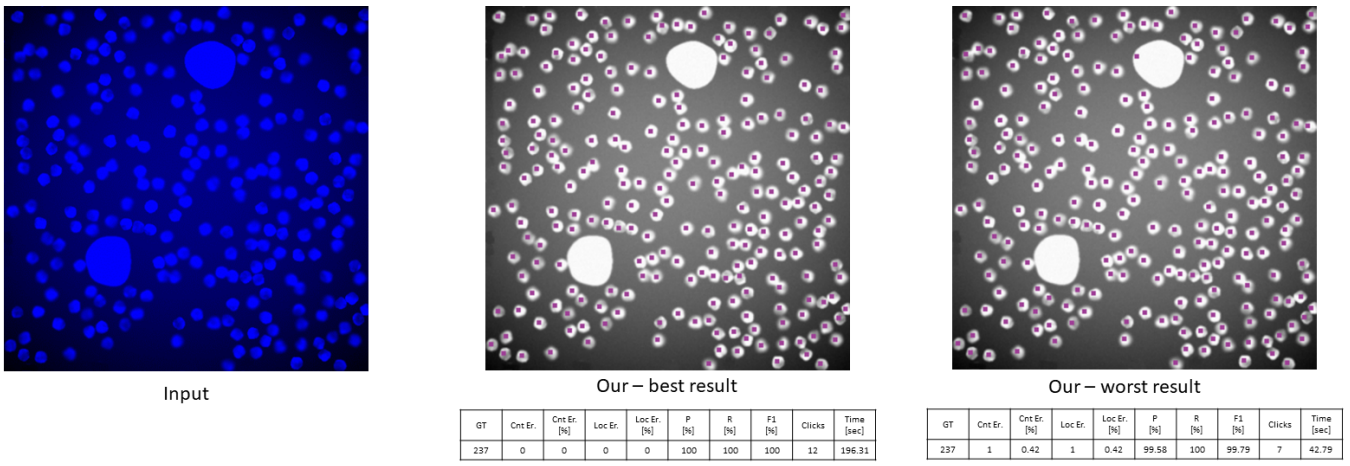


Figure 10: CellLrg. fluorescence microscopy cell images [4].

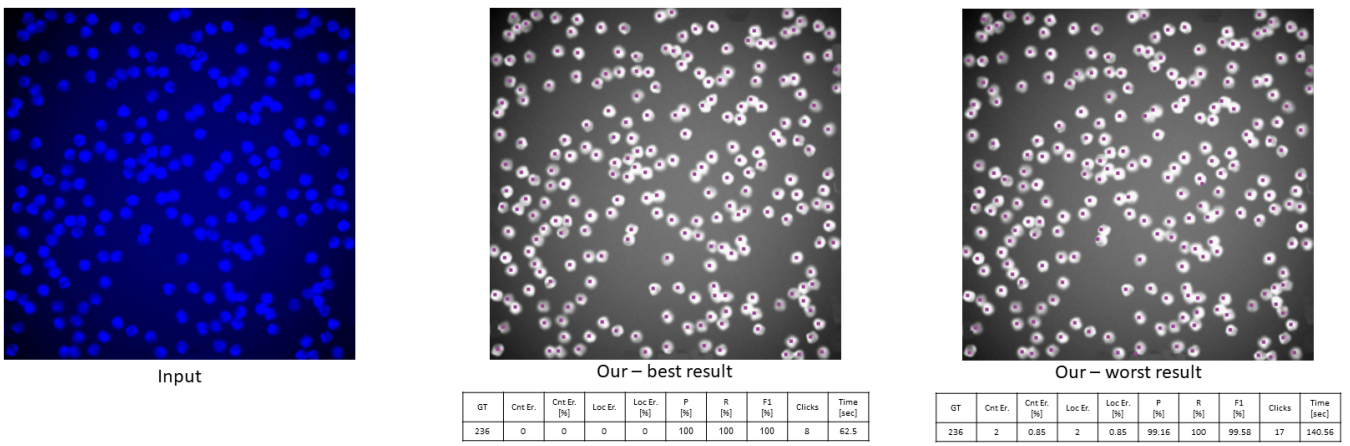


Figure 11: CellSml. fluorescence microscopy cell images [4].

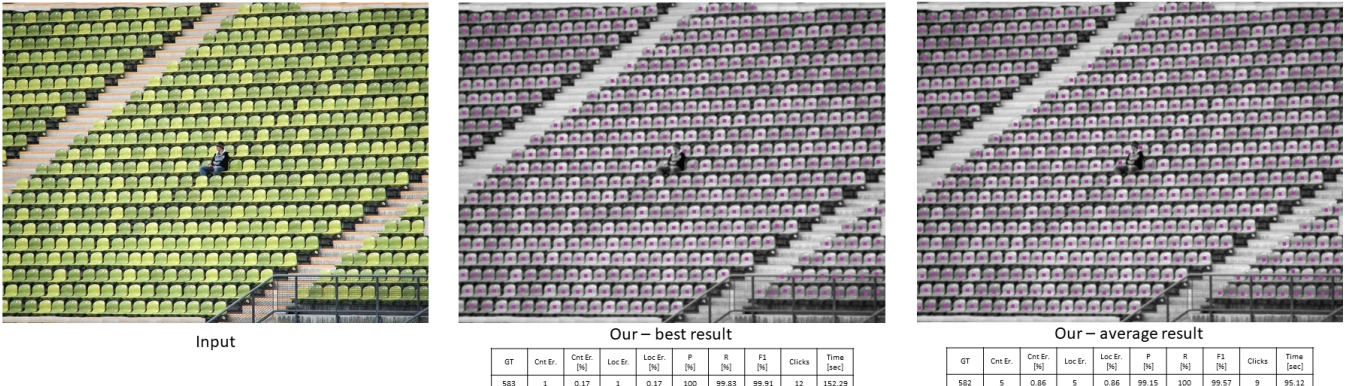


Figure 12: Chairs.

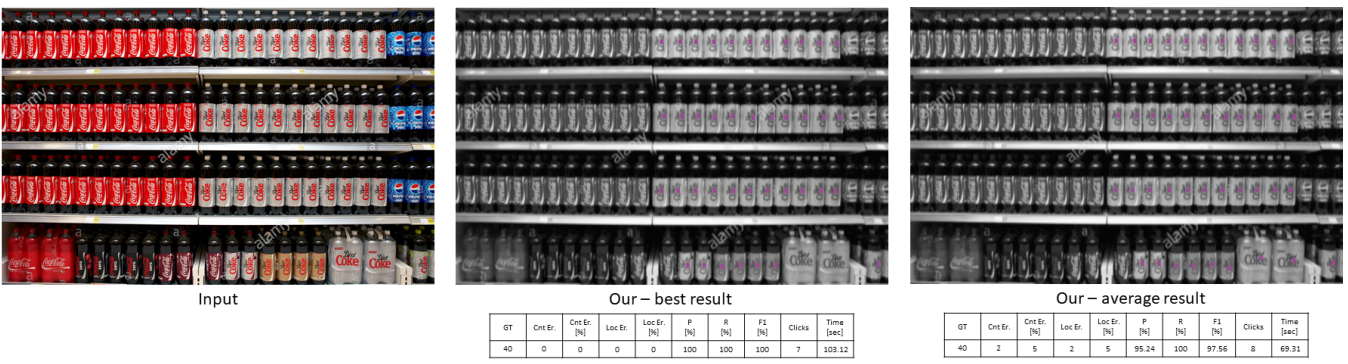


Figure 13: CokeDiet.

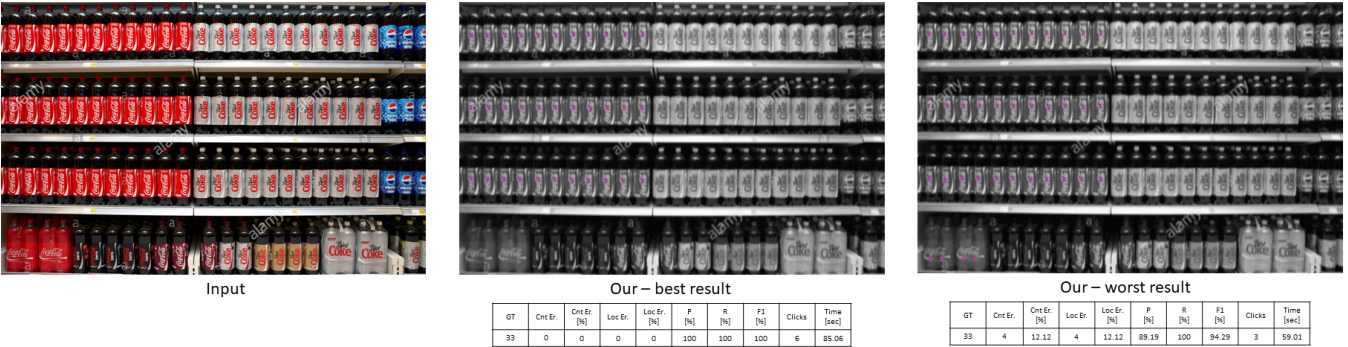


Figure 14: CokeReg.

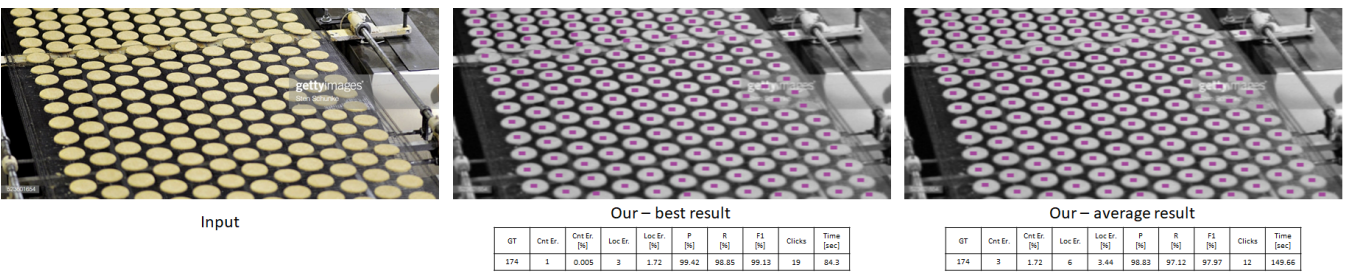


Figure 15: Cookies.

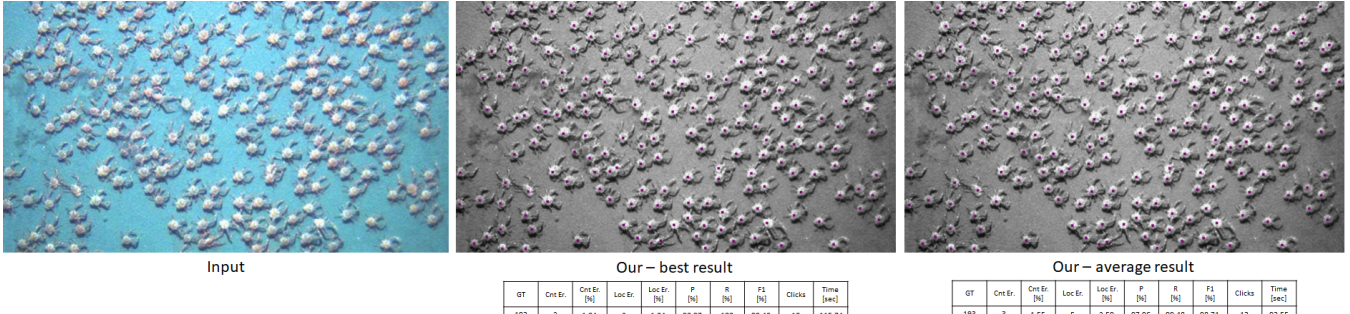


Figure 16: Crabs.



Figure 17: Crowd.



Figure 18: Discussion.

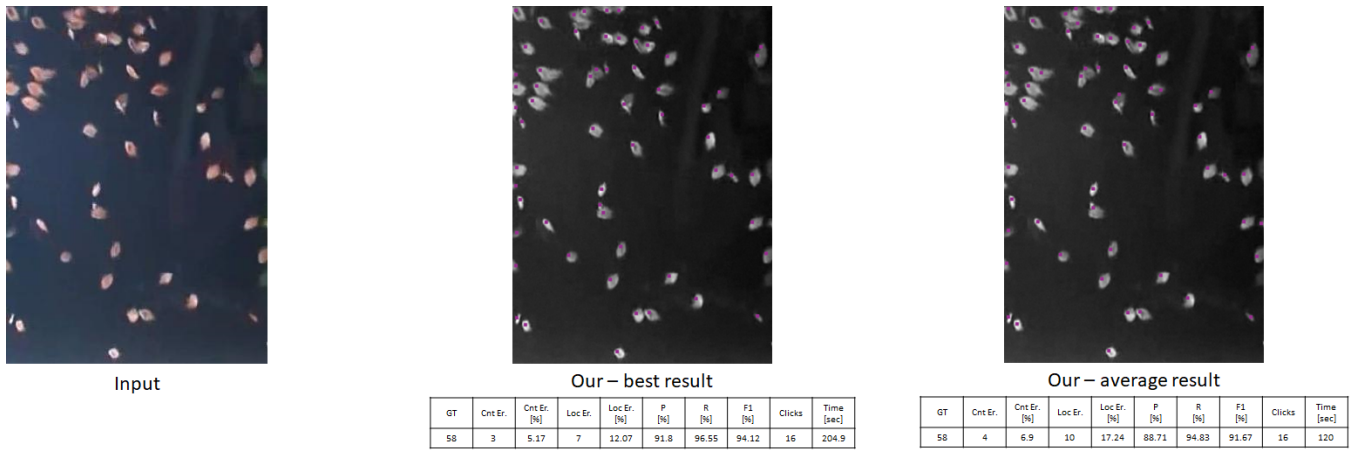


Figure 19: Fish097. small object dataset [5].

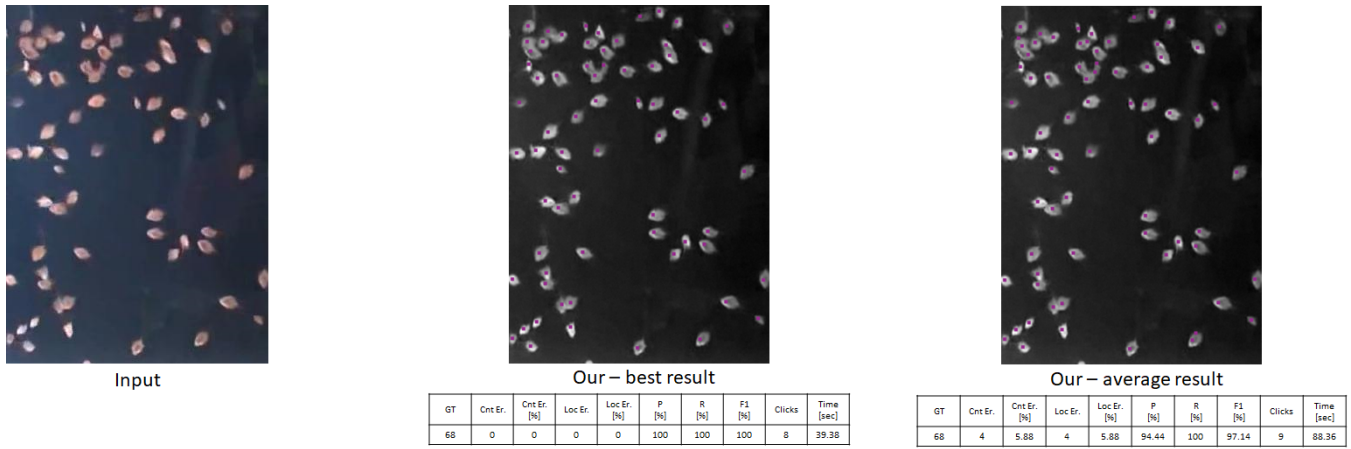


Figure 20: Fish107. small object dataset [5].

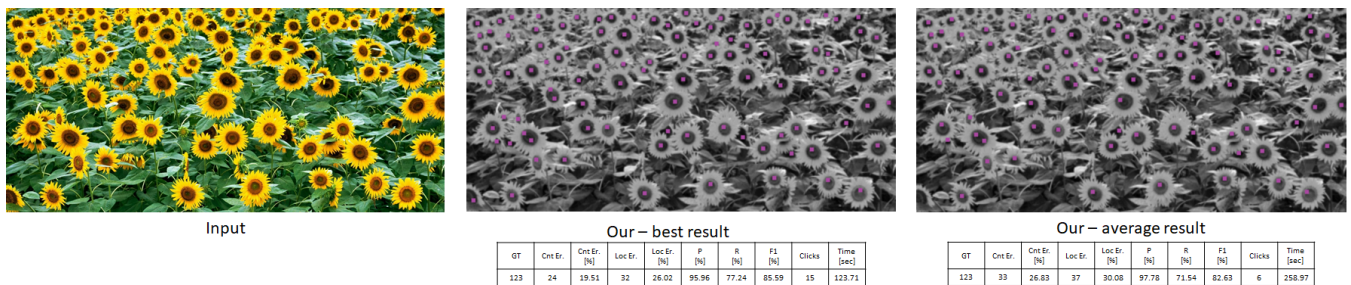


Figure 21: Flowers.

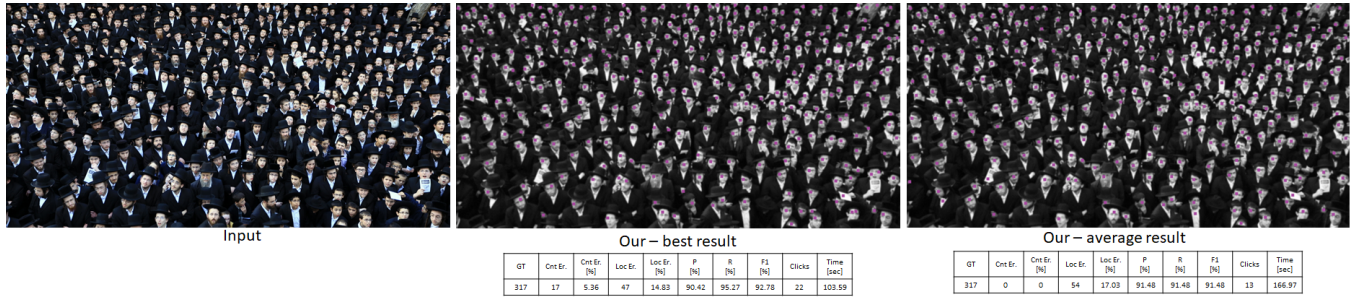


Figure 22: Hats.

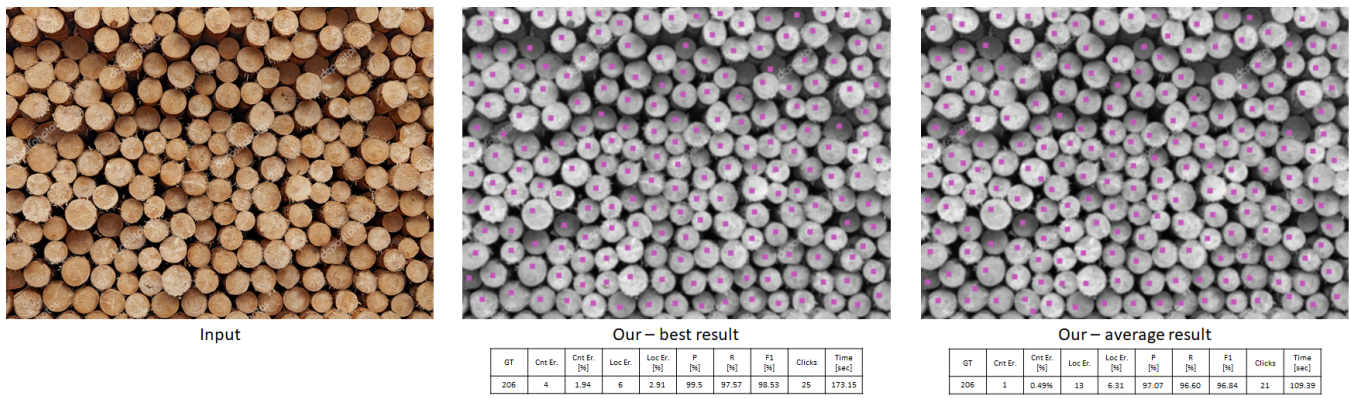


Figure 23: Logs.

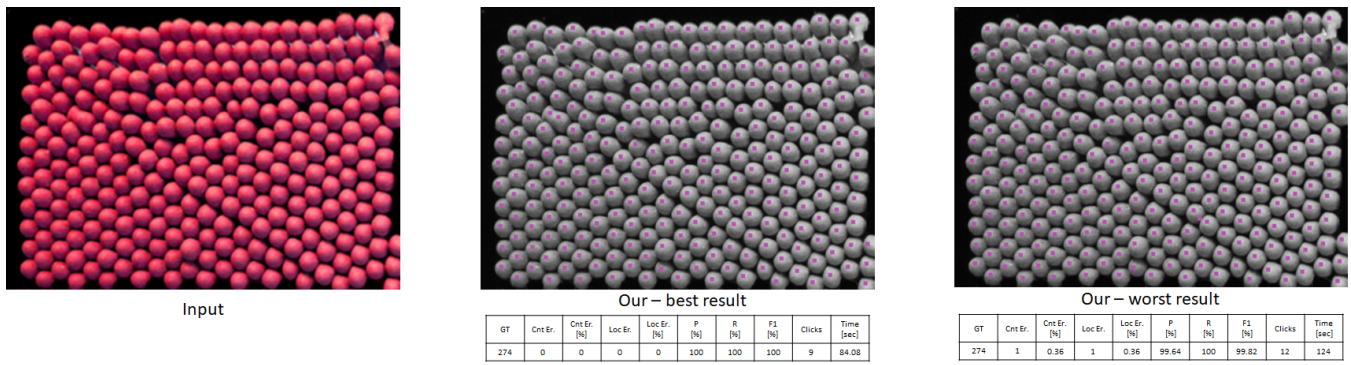


Figure 24: Matches.

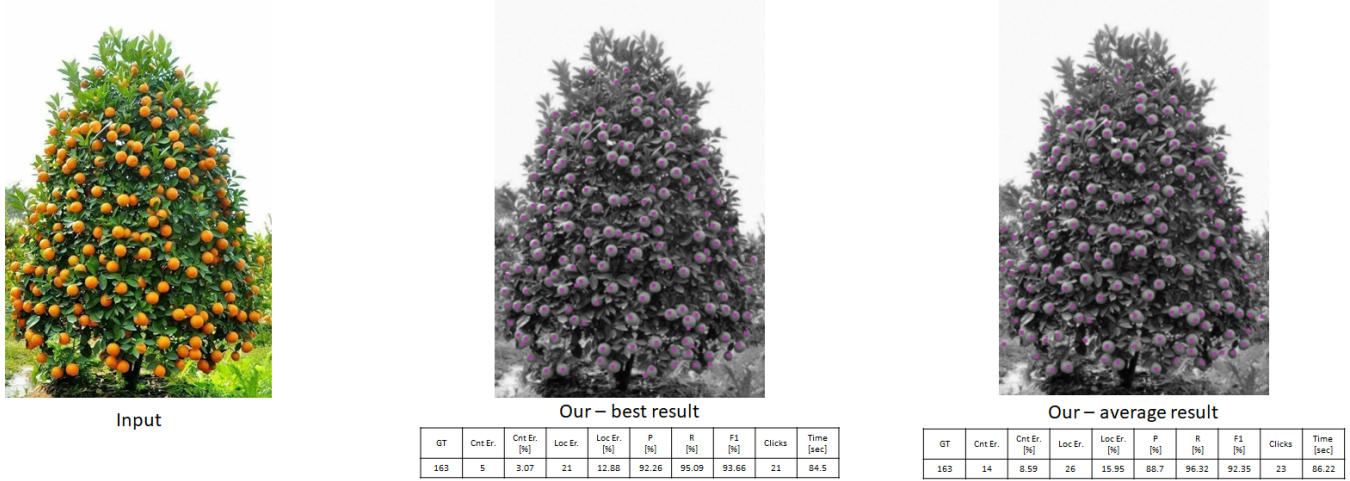


Figure 25: Oranges.

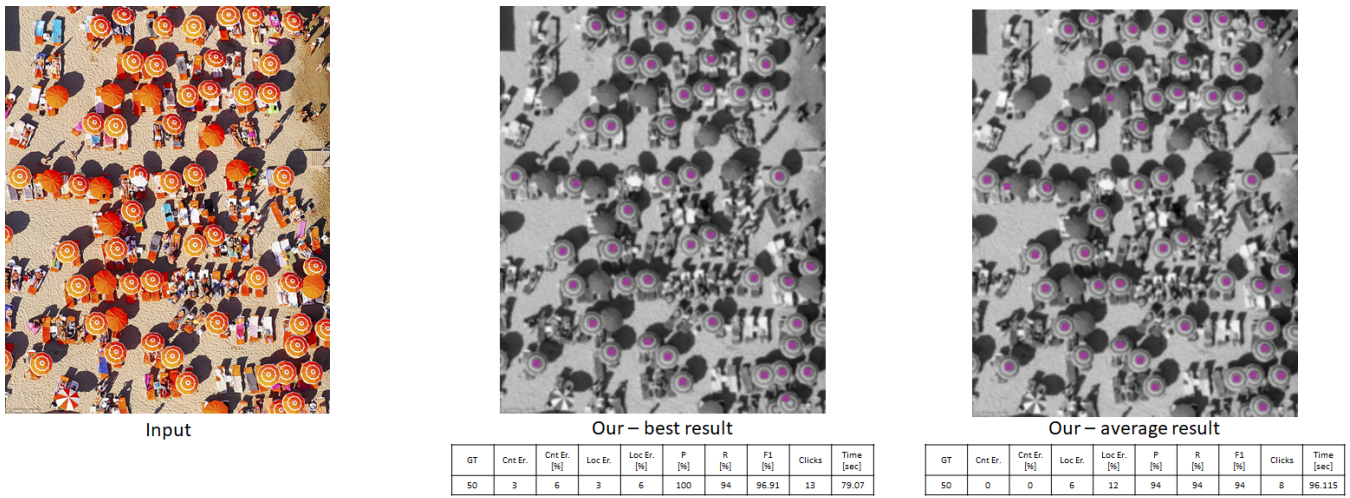


Figure 26: Parasol.

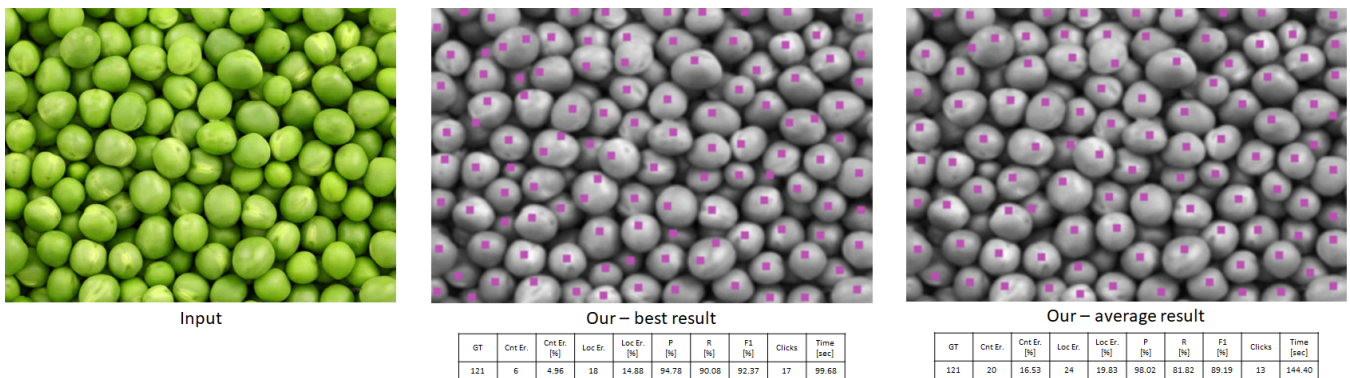


Figure 27: Peas.

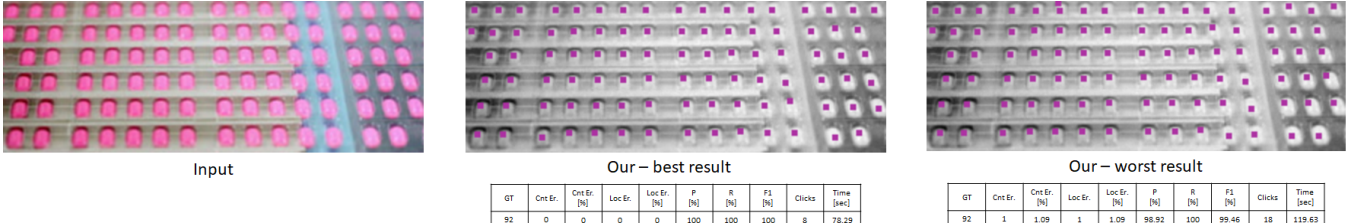


Figure 28: Pills.

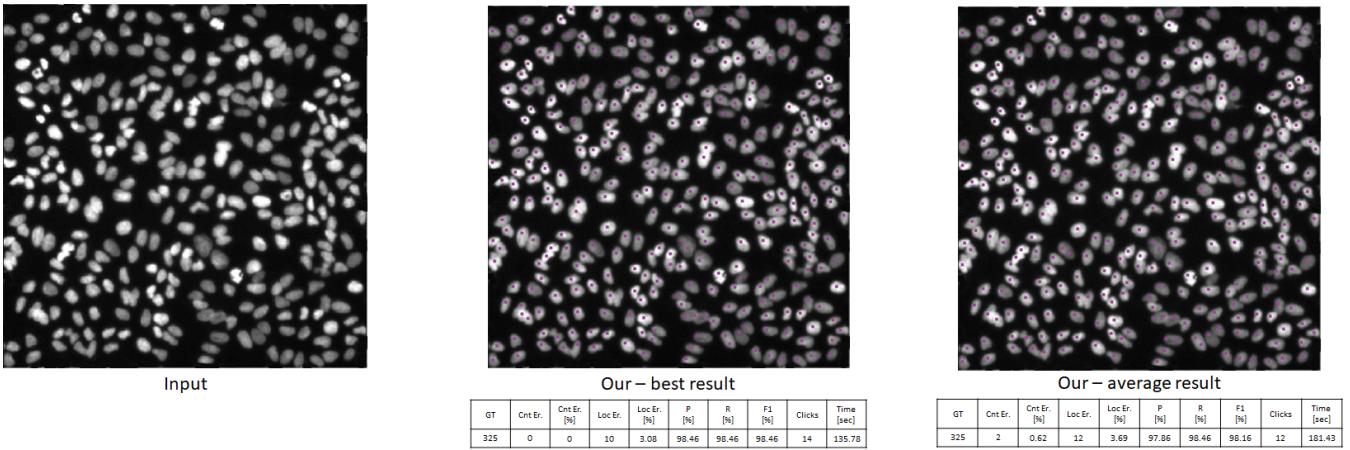


Figure 29: RealCells. Taken from [2].

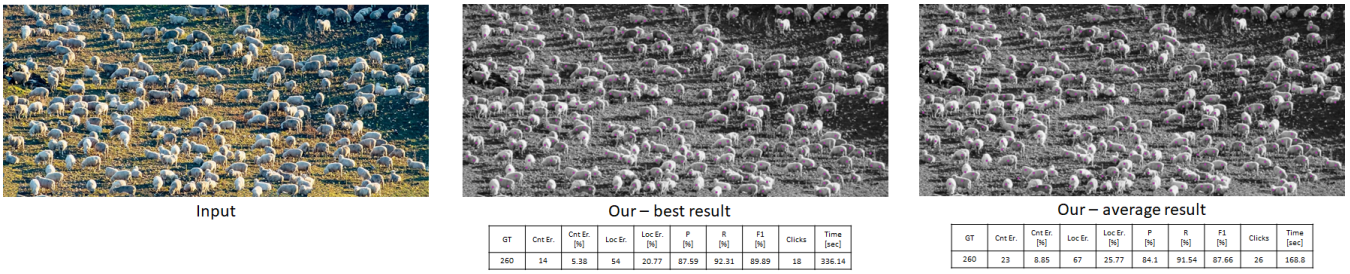


Figure 30: Sheep.

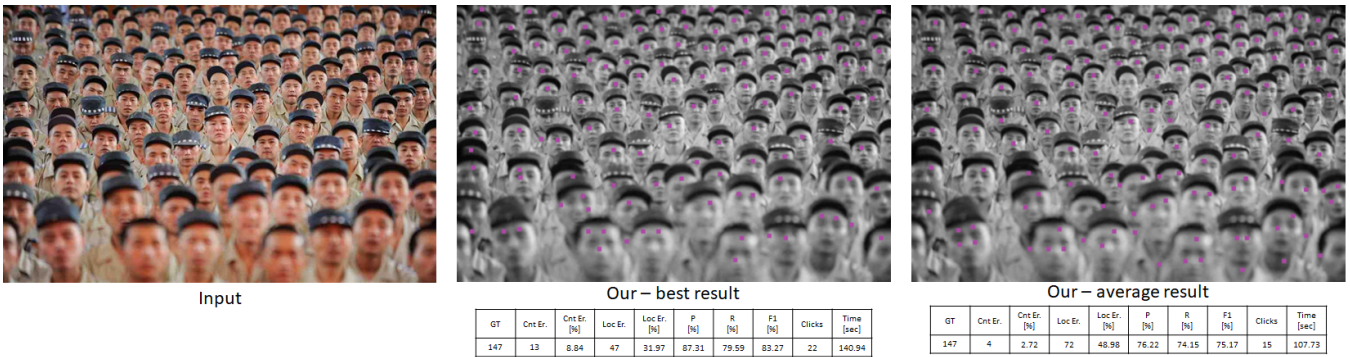


Figure 31: Soldiers. ShanghaiTech dataset [6].

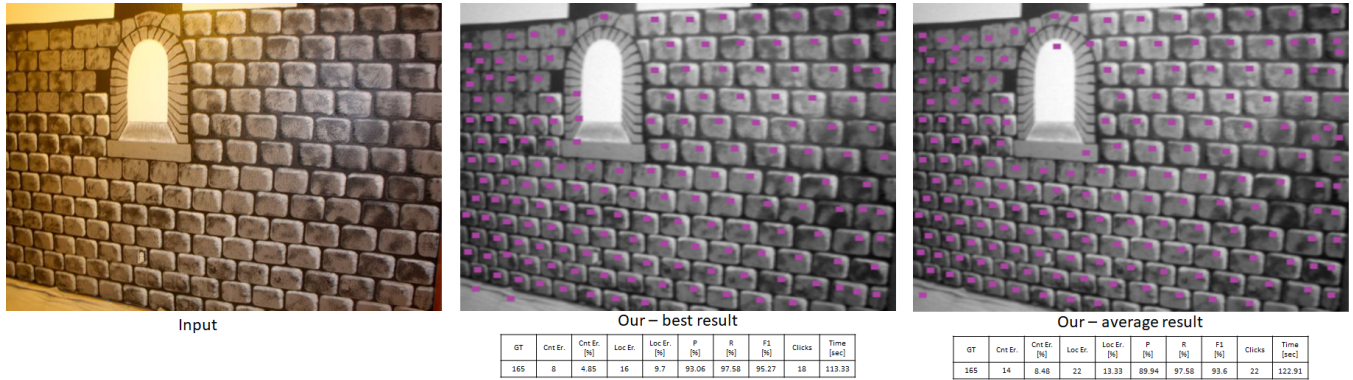


Figure 32: Wall.

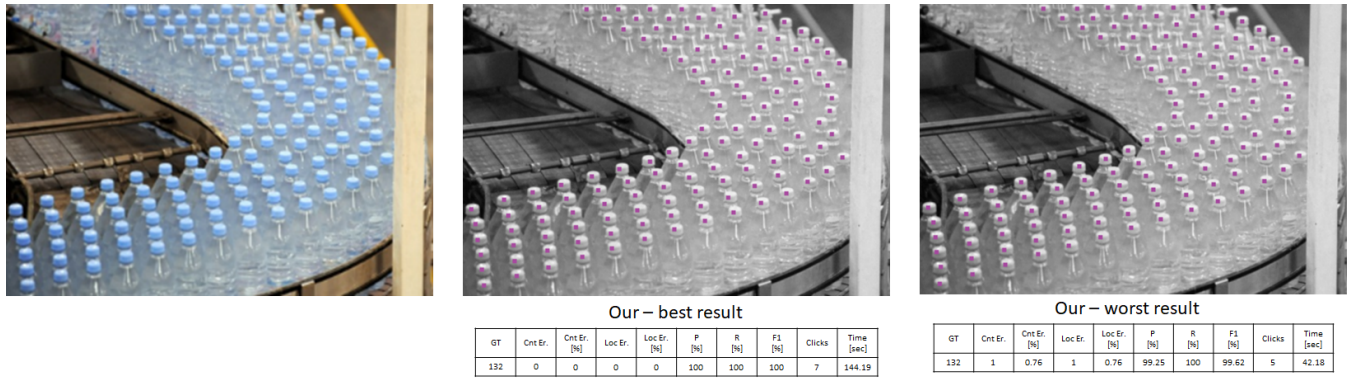


Figure 33: Water.

References

- [1] C. Arteta, V. Lempitsky, J. A. Noble, and A. Zisserman. Interactive object counting. In *European Conference on Computer Vision*, 2014. [9877](#), [9878](#)
- [2] Elena Bernardis and Stella Yu. Pop out many small structures from a very large microscopic image. *Medical image analysis*, 15:690–707, 07 2011. [9878](#), [9888](#)
- [3] Inbar Huberman and Raanan Fattal. Detecting repeating objects using patch correlation analysis. *2016 IEEE Conference on Computer Vision and Pattern Recognition (CVPR)*, pages 2903–2911, 2016. [9877](#), [9878](#)
- [4] Antti Lehmussola, Pekka Ruusuvuori, Jyrki Selinummi, Heikki Huttunen, and Olli Yli-Harja. Computational framework for simulating fluorescence microscope images with cell populations. *IEEE Trans. Med. Imaging*, 26(7):1010–1016, 2007. [9878](#), [9882](#)
- [5] Z. Ma, Lei Yu, and A. B. Chan. Small instance detection by integer programming on object density maps. In *2015 IEEE Conference on Computer Vision and Pattern Recognition (CVPR)*, pages 3689–3697, June 2015. [9878](#), [9880](#), [9881](#), [9885](#)
- [6] Yingying Zhang, Desen Zhou, Siqin Chen, Shenghua Gao, and Yi Ma. Single-image crowd counting via multi-column convolutional neural network. *2016 IEEE Conference on Computer Vision and Pattern Recognition (CVPR)*, pages 589–597, 2016. [9878](#), [9888](#)